WP8 DELIVERABLES / YEAR 2 (February 2003)

D 8.3

Coupled 3-D physical and biogeochemical model, applied on the Western Black Sea (model HB)

D 8.5

Seasonal distributions of physical and biogeochemical properties for the western Black Sea

J. Staneva[1], V. Kourafalou[2], K. Tsiaras[2] and E. Stanev[1]

[1] Department of Meteorology and Geophysics, University of Sofia, 5 James Bourchier Street, 1126 Sofia, Bulgaria; e-mail: joana@phys.uni-sofia.bg;

[2] National Center for Marine Research, Anavissos, 19013, Greece, villy@ncmr.gr

TABLE OF CONTENTS

1. Introduction

The Black Sea ecosystem has experienced several changes since the 1960s driven by several perturbations in the drainage basin of the rivers and the Black Sea itself. The man-made changes include land use; changes of hydrological regimes of out-flowing rivers; introduction of exotic species, as the gelatinous Ctenophore Mnemiopsys; and selective or excessive fishing. Given the different characteristics of these changes (for instance difference on impacts of land use changes among Si(OH), PO_4 and NO_3), we still do not know which are the most important ones in terms of large-scale biological and ecological consequences and what the synergy between the human activities and the natural forcing would be. Simple correlations based on current and historical ecological observations are not sufficient. The biogeochemical models provide a powerful tool for studying the biological and chemical compartments as a function of physical and human impacts. One of the main aims of the EU project **DANUBS** (**NU**trient management of the **DA**nube basin and its impact on the **B**lack **S**ea) is to study the recent eutrophication-related ecosystem changes in the Danube-Black Sea mixing zone. As a mathematical tool for studying those changes we use a hierarchy of hydrological end ecological models with different level of complexity and different time and space discretization. The effect of nutrient discharge on the quality of a given ecosystem is tested by looking at the seasonal variability of the transport of Danube-induced water and the behavior of the northwestern Black Sea shelf ecosystem.

The main aim here is to illustrate the basic physical and biological dynamics of upper ocean using mathematical models. The physical models with different complexity including mixed layer dynamics as the most important physical background for ecological system (Oguz et al., 1996; Staneva *et al.*, 1998, Oguz et al., 2001), or full set of primitive equations (Gregoire *et al.*, 1998, Gregoire et al., 1997) are used for providing the hydrodynamics in coupling of physical, chemical and biological processes in the Black Sea. The biological models with different trophic Black Sea ecosystem in relation to the first order physical effects within the mixed layer have been recently reviewed by Oguz et el. (1996) and Oguz et al., (2001), Van Eeckhout et al, (1998), Lancelot et al., (2002), etc. Simulations using low dimensional physical models are analyzed in the

above studies with a focus on the ecosystem response to the seasonal variability in atmospheric forcing. Recently, a low-tropic-level biological model was coupled for the first time with 3-D primitive equation model of the Black Sea, and the results were reported in the paper of Gregoire *et al.* (1997), Besiktepe et al., (2001).

The coupled computational integration system used here could be regarded as a tool for simulation of annual upper ocean dynamics and biogenic element cycle in response to changes in the physical systems and river-induced water transports of nutrients. Thus, unlike some previous studies, the present one aims to answer the question to what extend the stratification and the discharge from the Danube River affects mixing processes and in particular the behavior of a coupled physical-biological model. Estimates on the spatial variability of the biological system simulated by the 3-D coupled model are also given. All models used here are summarized in Table 1.

The hydrodynamic models are based on the 3-D Princeton Ocean Model (POM) applied for the western Black Sea in fine resolution (~5 km grid) and on the entire Black Sea in coarse resolution (~10 km grid); and the 3-D hydrodynamic model (MOM), applied for the whole basin, in coarse resolution (~10 km grid). The basin-wide MOM provides the air-sea interaction fields and climatological temperature and salinity fields. The basin-wide POM inserts plume dynamics in the MOM initial fields, plus boundary conditions for the fine grid northwestern POM application, which is the hydrodynamic part of the coupled shelf model POM-BIO, described below. The detailed description of the hydrodynamic models is given in the deliverables D8.1 and D8.2 respectively. Here we describe briefly in Section 2 the basic models, as well as their initial and boundary conditions. One of the main physical characteristics governing the biological processes is the mixed layer at the upper layers. Therefore it is of crucial importance to simulate correctly the mixed layer depth variability. The mixed layer model is described in Section 2.1. The ecological models are based on Fasham-like model (Fasham et al., 1990, section 3.1) and the European River System Ecological Model (ERSEM, section 3.2). The different strategies are using for this coupling depending on the complexity of the trophic level Black Sea ecosystem and the model discretizations.

In general, the decision support system is based on the integration of management, modern information technology and innovative modeling methods. The mathematical

models lie in the heart of such a system. The choice of the models by the scientific community depends on both: (i) their completeness for the describing the required processes and (ii) their validity. This is the base of the fundamental question in the environmental modeling. The more complete (more complex) a model is, the more difficult it is to validate it and the slower and the more uncomfortable it is to handle. The freedom in such a model is very high and its calibration depends upon the available data and knowledge. The observational data normally are sparse in time and space. Therefore the statements "reliable" and "fast" cannot be implied simultaneously into a decision-supporting tool. This conception lies into the base of the modeling work package wp8. We have developed a hierarchy of models that can be easily adjusted and applied for different simulations, as dictated by the management needs. The model data flow and characteristics are shown in Fig. 1 and Table 1.

A direct "on-line" coupling is perform between the low trophic ecological model based on the variability of the phytoplankton and nutrients (Fasham, 1990, Staneva et al., 1998, Oguz et al., 1996, see Section 3.1) and the 3-D fine resolution hydrodynamic model (POM) for the north western Black Sea (we will refer it further as POM-BIO). In POM-BIO the climatological monthly fields of temperature and salinity are relaxed by the ones diagnosed by the coarse resolution basin-wide 3-D hyrdrodynamical model (MOM). A detailed description of these fields is given in section 4.2. In addition, some results from the coarse resolution basin-wide Black Sea model (MOM-BIO) are also presented (see section 5.3). The model uses atmospheric analyses data and a flux parameterization based on bulk formulation to diagnose the surface wind stress and fluxed (see Section 2.3). These fluxes are further used for boundary conditions by POM-BIO. A description of the horizontal and vertical distribution of POM-BIO is given in section 5.1. "Off-line" coupling with ERSEM is further performed (MLD-BIO). In order to include the most important ecological and physical processes associated with the impact of the Danube River this coupling uses the model physics diagnosed by the POM-BIO, mixed layer dynamics (see Section 2.1) and complex ecological model ERSEM (See Section 3.3). The evolution of the vertical profiles of some of the biogeochemical variables is described in Section 5.2.

In the next year, real simulations with the mathematical models have to be performed. The POM-BIO model will be further validated with the aim of observations, based mainly on the SeaWiFS satellite images. MLD-ERSEM will use the data from wp5 and wp7 for both initial and boundary conditions and validations.

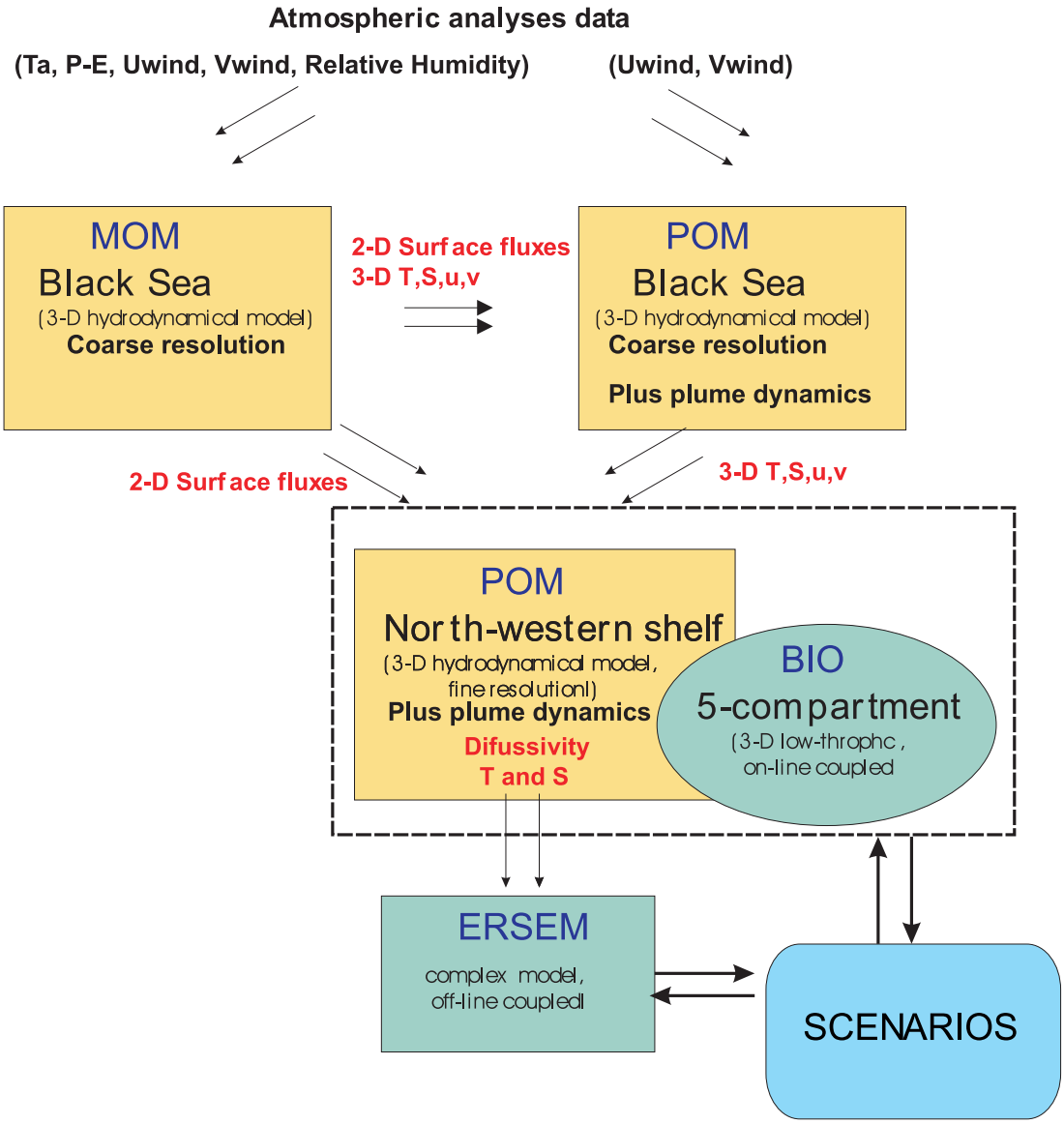

Fig. 1: Schematic of model simulations connectivity and data flow.

2 Physical models

2.1. Mixed layer model

The mixed layer routine is based on the formulation of Gill and Turner (1976). The major assumptions of the model (Gordon and Bottomley, 1985) are: (1) all surface heat flux is used to heat/cool the column, all fresh water flux modifies the salinity, and all other tracer fluxes modify the corresponding tracer values; (2) all the kinetic energy available for mixing is used to increase the potential energy of the column; and (3) mixing is instantaneous (i.e. acts on shorter time scales than the model time step). The model is based on the principles of energy conservation; hence we define below the heat content of the mixed layer H, and the potential energy.

The mixed layer model works in several stages: (1) increment of tracers with profile, derived from surface fluxes and depletion of mechanical energy; (2) determination of density changes arising from changed tracer profiles, and calculation of the energy, required to mix each layer internally (i.e. the work done to increase its potential energy); (3) mixing tracers between layers if (a) the two layers are unstable, or (b) there is mechanical energy available to mix between stable layers.

This model relates changes in the potential energy of a vertical water column to the rate of working by the momentum. The rate of turbulent energy input at the surface due to wind forcing

$$W=\mu\rho_w v_*^3$$

where v_* is the ocean friction velocity, ρ_w is the density of sea water, and μ is a scaling factor of the order of unity. This is decayed exponentially with depth to prevent overdeepening of the mixed layer in winter. It is used further to mix the surface heat input throughout the mixed layer. Convection in the model is partly penetrative with 85% of convectively generated turbulent kinetic energy dissipated within the mixed layer. The penetrative short wave flux is represented by a double exponential decay function (Paulson and Sympson, 1977).

The forcing functions of the mixed layer model are: the penetrative (solar) component of surface flux, the non-penetrative heat flux (this contributes to the heating of the top layer) and the mechanical ("wind mixing") energy, which is available for

mixing water in the stably stratified column. We give below a short description of physical forcing. It is described in details in section 2.4.

2.2 Modular Ocean Model (MOM)

The model set-up for the Black Sea follows Staneva and Stanev (1997) and Stanev and Staneva (2000). It employs the modular ocean model (MOM) version of Bryan-Cox-Semtner model (Bryan, 1969, Pacanowski *et al.*, 1991). The model has a horizontal resolution of $1/12^0$ in latitude, $1/9^0$ in longitude (almost square grid elements with grid intervals of about 9 km). The bottom topography is taken from the UNESCO bathymetric map and discretized with the model resolution. We have 24 levels, the thickness of layers varying from 5 m in the surface 20 m, 10 m until 90 m, decreasing to 400 m in the deep homogeneous layers and increases again to 60 m in the deepest levels.

The atmospheric forcing (temperature, relative humidity and winds at sea surface) is prepared from the twice-daily atmospheric analysis data produced in Hadley Center, United Kingdom Meteorological Office (UKMO). Sea surface salinity is relaxed to climatological data, which are calculated at every model time step from monthly mean data. The salt balance in the model is closed at the Bosphorus Straits by continuously adding a positive salinity flux. This flux is calculated from the diagnosed salinity flux at the sea surface, using a simple physical model for water exchange in the Straits (Stanev *et al.*, 1997, Staneva and Stanev, 1998). The results of observations and the hydraulic control theory enable us to parameterize the strait inflow as a function of water balance at the sea surface. The parameterization is fitted to observations (Unluata *et al.*, 1989, Oguz *et al.*, 1990). To simulate realistic convection in the Bosphorus Straits area, a routine, parameterizing the plume and the entrainment is added to the main code. Details on the model sensitivity to different parameterizations are given by Stanev *et al.* (1997). The vertical mixing is tuned against the independent data of Lewis and Landing (1991) based on measurements of manganese and iron in the Black Sea. The subgrid parameterizations include biharmonic mixing and diffusion in the horizontal. The coefficients are the same as in the works of Staneva and Stanev (1997) and Stanev and Staneva (2000). The bottom is insulating:, where Kv is the coefficients of vertical diffusion.

The simulations of circulation model are analysed by Staneva and Stanev (1997)

and Stanev and Staneva (2000). The water mass formation in studied in Staneva and Stanev (2002).

2.3 Princeton Ocean Model (POM)

The Princeton Ocean Model (*Blumberg and Mellor, 1983)* is a 3-dimensional, primitive equation, free surface and sigma-coordinate hydrodynamic model. The model has been modified to include river plume dynamics, following the approach developed by *Kourafalou et al.* (1996a), where a source term is added in the continuity equation, representing the volume of the river input. This approach allows for the numerical description of the phenomena associated with river runoff, based on model input of the river discharge rate and the salinity of the incoming water. The value of salinity near the mouth is thus time and space varying and determined according to the mixing conditions. The code used here has been further modified to allow for the specification of temperature for the incoming river waters, as in *Kourafalou* (1999).

The horizontal mixing depends on the grid size and the velocity field, as the horizontal eddy viscosity / diffusivity parameter is given by the Smagorinsky formula. The vertical eddy viscosity / diffusivity parameter is calculated according to the *Mellor and Yamada* (1982) turbulence closure scheme, which solves the equations for turbulent kinetic energy and turbulence macroscale and provides a realistic simulation of the mixed layer taking account of the wind stirring and the stability induced by stratification. In the vertical the model uses a bottom following sigma coordinate system. Thus all vertical levels are maintained throughout the model domain permitting a better resolution of the bottom boundary layer, which is particularly suitable for coastal regions where bathymetric effects are important. The model can successfully represent the dynamics of a freshwater plume, as was shown in previous studies of river plumes, in semi-enclosed Mediterranean basins (*Kourafalou*, 1999, 2001) and in the open ocean (*Kourafalou et al.* 1996b).

The model domain lies between 27.71^{o} and 33.60^{o} East and 41.03^{o} and 46.61^{o} north. Horizontal resolution of the model is ~5Km. Sixteen sigma-levels are resolved in the vertical, with logarithmic distribution approaching the surface in order to achieve a better resolution of the upper layer. Realistic bathymetry is used and minimum depth is

set to 5m.

The river sources are represented by an 8-point source for Danube, a 2-point source for Dnepr and single point sources for Bug and Dnestr rivers. River runoff for all rivers except Danube has been set to constant values (500m^3/s Dnepr, 300 m^3/s Dnestr, 100 m^3/s Bug). Danube's discharge rate is varying according to the climatological data prepared by daNUbs wp7 and the daily data provided by wp5 (A. Constantinescu, Pers. Comm.). We have also included the input of nutrients from Danube's runoff based on climatological data (monthly averages) from wp7 (A. Cociasu).

The initial conditions for the biological state variables were obtained with a density dependent interpolation from the vertical profiles previously simulated by a 1-D version of the coupled model. Using density rather than depth for the interpolation into the model grid is aiming at the exclusion of variability due to dynamical effects (Gregoire et al.-1997, Turgul et al.-1992, Saydam et al.-1993). Starting time was set to 1 September.

The values of biological variables along the open eastern boundary are calculated from a density dependent area average over the open sea. An alternative is to use the fields produced by a large scale coupled model over the entire Black Sea.

2.4 Boundary conditions

The net heat flux at sea surface can be represented as:

$$Q^T = Q_s - Q_u \quad , \qquad (1)$$

where Q_s is the downward flux of solar radiation and Q_u is the net upward flux of radiation emitted by the sea surface via radiative and evaporative-conductive processes.

$$Q_u = H_a + LE_a + Q_b$$

The net upward flux includes the net flux of long wave radiation loss Q_b, sensible H_a and latent LE_a heat flux (L=2.501.10^6 $J\ kg^{-1}$ is the latent heat of vaporization). For the long wave radiation loss we use the formulae of Berliand and Berliand (1952), modified as in Rosati and Miyakoda (1988), and for the sensible and latent heat flux the following bulk formulae:

$$H_a = \rho_a C_p C_h |W| \times (T_s - T_a) \quad , \qquad (2)$$

$$E_a = \rho_a C_e |W| \times \left[e_{sat}(T_s) - r\, e_{sat}(T_a) \right] \frac{0.622}{p_a}$$

, (3)

where: T_s and T_a are the SST and the atmospheric temperature at 1000 mb respectively, $e_{sat}(T_a)$ is polynomial approximation, r_a is the density of the air, p_a is the surface air pressure (p_a=1013 mbar), $|W|$ is the surface wind magnitude, C_p is the specific heat capacity ($C_p = 1.005 \times 10^3$ J [kg.K]$^{-1}$), C_h, C_e are turbulent exchange coefficients.

Wind stress is parameterized as:

$$(\tau^{\lambda}, \tau^{\varphi}) = \rho_a\, C_d\, |W|\, (W_x, W_y) \quad (4)$$

where W_x, W_y are the wind components, C_d is the drag coefficient. Turbulent exchange and drag coefficients are assumed to be equal and dependent on the stratification in the boundary layer (Hellerman and Rosenstein, 1983, see also Staneva and Stanev, 1995). Momentum and heat fluxes are calculated interactively. The fractional cloud cover is inferred at each model step from the monthly mean data (Sorkina, 1974). The value of T_s in the parameterizations for the wind stress and for the net upward flux is set to be equal to the current SST, simulated by the mixed layer model. .

3. BIOLOGICAL MODELS

We have employed two biological models with different levels of complexity. The models are described below.

3.1 Low-trophic ecosystem model

A five-compartment biological model, which is based on the Fasham model (Fasham et al, 1990), has been tuned to the Black Sea conditions (see Staneva et al., 1997 and Oguz et al. 1996). The model has the following biological variables: phytoplankton biomass P, herbivore biomass Z, detritus D, nitrates N and ammonium A. There are some differences in our model from the one of Oguz et al. (1996), concerning the food-web functions, parameterizing the zooplankton grazing and mortality. These were tuned with data from observational evidence for the Black Sea conditions. The local changes of biological variables are expressed by sum of physical and biological parts:

$$dB/dt=(dB/dt)_{phy}+(dB/Dt)_{bio}\,. \qquad (5)$$

For the physical terms we use the same equations, as for temperature and salinity. The interactive functions for the biological components are described by Fasham et al. (1990). The parameter set is taken from the study of Oguz et al. (1996) and Staneva et al., (1998). The rate of change due to biological processes $(dB/dt)_{bio}$ is calculated separately from the physical part, thus we split the model in different processes. In the equation of detritus and zooplankton we add additional terms, which describe the grazing of detritus by herbivore (S. Moncheva, personal communication).

3.2. ERSEM

The European Regional Seas Ecosystem Model (ERSEM), Baretta et al. 1995, consists of five modules (conceptual units): Primary producer module; Microbial loop module; Mesozooplankton module; Benthic nutrients module and Benthic biology module. State variables in ERSEM have been chosen in order to keep the model relatively simple without omitting any component that exerts a significant influence upon the energy balance of the system. The dynamics of biological functional groups are described by both physiological (ingestion, respiration, excretion and egestion) and population processes (growth, migration and mortality). Detailed descriptions of the biological sub-models can be found for: phytoplankton in Varela et al. (1995); Ebenhöh et al. (1997); functional groups related to the microbial food web in Baretta-Bekker et al. (1997); mesozooplankton in Broekhuizen et al. (1997); fish in Bryant et al. (1995) and benthic fauna in Ebenhöh (1997); Blackford (1997). The dynamics of biological functional groups are described by both physiological (ingestion, respiration, excretion and egestion) and population processes (growth, migration and mortality). The ecosystem in the ERSEM is subdivided into three functional types: producers (phytoplankton), decomposers (pelagic and benthic bacteria) and consumers (zooplankton and zoobenthos).

The conceptual structure of the model is presented in Fig. 2

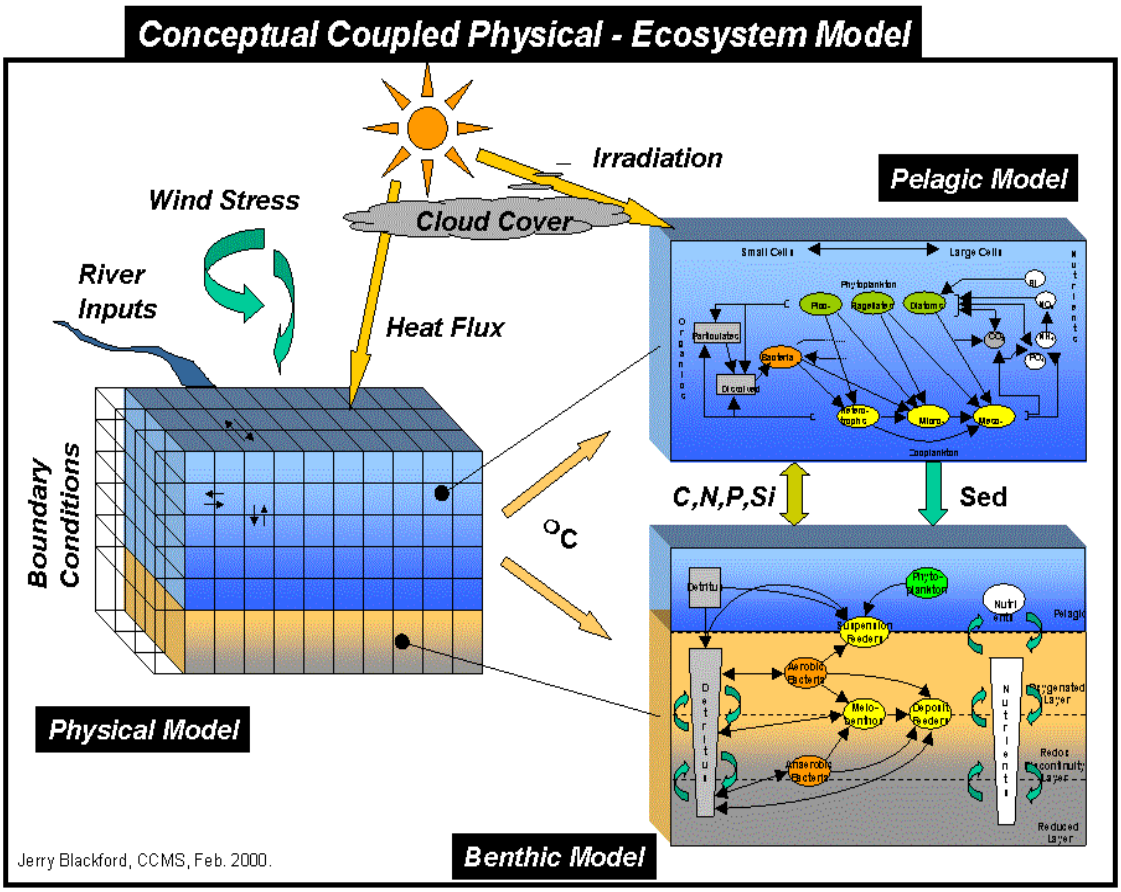

Figure 2: Conceptual structure of the ERSEM

The evolution of the vertical profiles of temperature and salinity are taken from the diagnostics from POM. The area and depth of the column do not change with time. The momentum and heat fluxes used to force the mixed layer model are calculated interactively at each time step using the same techniques as described in Section 2.4. The initial conditions for temperature and salinity are taken from POM-BIO simulations. In addition the physical variables are relaxed to those obtained by POM-BIO. The vertical diffusion coefficients are calculated by the mixed layer model. We assume zero sea surface fluxes from the biogeochemical state variables.

4. Seasonal distribution of the physical properties.

4.1. Mixed-Layered Dynamics

The performance of the 1-D physical model is illustrated by Fig. 4.1.1 and Fig. 4.1.2 (Figures Group 1). It shows the time evolution of the depth of upper mixed layer and predicted sea surface temperature for the open Black Sea area. The symbols displayed at each graph correspond to the data from observations. It is clearly seen that there is quite a good agreement between the data from the observations and the model results. The seasonal evolution of the vertical profiles of temperature and salinity in the open area is shown on the in Fig. 4.1.2. The predicted thickness of the upper mixed layer fluctuates seasonally between 5 and 60 m. The convective mixing is maximal at the end of February, displacing the mixed layer depth (MLD) up to about 60 m reaching 6.5-7.0 ^{o}C (see Fig. 4.1.2). The permanent pycnocline maintained by the strong dilution of sea surface water (with salinity of about 18 psu) and the inflow of dense Mediterranean Sea water through the Bosphorus strait (with salinity of 35 psu) prevent deeper winter convection. The maximum temperature at the sea surface (about 24 ^{o} C) is observed during summer. The cold intermediate layer (CIL) is formed during winter and does not disappear throughout the year.

4.2. Three-dimensional hydrodynamic model MOM (rigid lid surface, no plume dynamics) applied on the Black Sea (coarse resolution)

In this section we present the seasonal distribution of the basic physical properties diagnosed by the 3-D hyrodynamical model for the Black Sea. The model is described in deliverable D8.2 and briefly in Section 2. The model performance and the comparisons between the model and data are analyzed in detail in D8.2

Seasonal and monthly mean heat flux distribution diagnosed by the model is shown on Fig. 4.2.1 and Fig. 4.2.2 (Figures Group 2). The minimal values of the heat flux during the winter (Fig. 4.2.1a, 4.2.2a) are simulated in the northeast part of the sea (about -180 W/m^2), the maximal values in this period of the year are about 0 W/m^2 (along the

west coast and the south-western and south-eastern parts of the basin). The heat flux starts to increase in the spring months (Fig. 4.2.1b, 4.2.2b, 4.2.2c) and reaches its maximal values along the eastern coast - above 200 W/m^2. In summer (Fig. 4.2.1c, 4.2.2d) the heat flux is minimal in the shelf area. Similar feature is also observed in the autumn (Fig. 4.2.1d, 4.2.2e, 4.2.2f). These results correspond very well with the climatological observations (see also Staneva and Stanev, 1998).

The seasonal and monthly mean wind stress distribution is illustrated in Fig. 4.2.3 and Fig. 4.2.4. The wind stress has two areas of maximal values during the whole year- in the western south-eastern (the area of Bitumen eddy) parts of the sea. The highest values are simulated during the autumn and winter-of about 0.45-0.55 N/m^2. The lowest values are observed in the central part of the basin.

Seasonal and monthly mean distributions of the temperature are shown on figures 4.2.5-4.2.18. In winter the lowest temperatures at the sea surface are simulated in the shelf zone (of 1 ^oC in February, Fig. 4.2.6a), the sea surface temperature increases in southern and southeastern directions and reach maximums at the easternmost part of the sea. The highest temperatures in summer (about 23 ^oC) are simulated along the coastal regions. The horizontal patterns of temperature at depth 75 m (Fig. 4.2.7, fig. 4.2.8) almost do not change during the year. Here we would like to remind that this is the depth within the Cold Intermediate Layer (CIL, a layer between 50 and 90 m, in which the temperature is below 8 ^oC through the whole year). There are two areas of local maxima at the western and central part of the basin, characterized with cyclonic circulation. The lowest temperatures are simulated in the shelf zone (This coincides with the observational evidence given by Ovchinnikov and Popov, 1987; Ovchinnikov, 1998; and Ivanov et al, 1997). Below the CIL (240 m, Fig. 4.2.9, Fig. 4.2.10) the distribution of temperature is very homogenous.

On figures 4.2.11-4.2.18 we present temperature cross-sections at 42.5 ^oN (Fig. 4.2.11, Fig. 4.2.12), 45.5 ^{o} N (Fig. 4.2.13, fig.4.2.14), 31.5 E ^{o} (Fig. 4.2.15, Fig. 4.2.16) and 38 E ^{o}(Fig.4.2.17, fig. 4.2.18). The cross-sections along the central part of the basin illustrate some of the main features of vertical stratification of the basin. CIL is well traced during the whole year. On the zonal and meridional cross-sections along the shelf zone the formation (45.5 ^oN) and the penetration (31.5 ^oE) of the cooled shelf water into

the basin interior are well seen. The formation of cold waters starts in the autumn and continues in the winter. The cooled water spreads all over the sea (fig. 4.2.15, 4.2.16).

Seasonal and monthly mean salinity distributions diagnosed by the model are presented on figures 4.2.19-4.2.32. The salinity at the sea surface (Fig. 4.2.19, 4.2.20) is about 18 psu and tends to increase in the interior of the Black Sea, due to the cyclonic circulation, which brings saltier waters from below. In the north-west part of the sea, the salinity is very low, due to the Danube freshwater discharge. The lowest salinity is observed in spring when the river runoff reaches its maximum. Salinity increases slowly with the depth. The higher values at all levels are simulated in the interior of the basin in the cyclonic areas. The lowest values in the deeper levels are in the south-eastern part in the area of the Batumi eddy. The cyclonic areas are well resolved also in the zonal cross-sections There is a strong horizontal gradient of the salinity patterns in the shelf zone (Fig. 4.2.27, 4.2.28), similar to the temperature ones.

Seasonal and monthly mean distributions of the velocity magnitude are shown on Figures 4.2.33-4.2.46. The maximal values of the velocity on the sea surface are associated with the main cyclonic current (rim current) of the Black Sea, and the anticyclonic eddy in the Batumi region. The patterns remain almost the same at 75 m (Fig. 4.2.35, 4.2.36), but the magnitude of the velocity decreases.

4.3. Three-dimensional hydrodynamic model POM (free surface and plume dynamics) applied on the Black Sea (coarse resolution) and on the Western Black Sea Shelf (fine resolution)

We describe the climatological hydrodynamic simulation that includes plume dynamics and formed the basis for the western Black Sea coupled physical and biological simulations. The results are monthly averaged fields of hydrodynamic fields that are uploaded in the DANUBS server; examples are illustrated in Figures Group3.

Forcing

A 2-year data base (wind stress and heat fluxes of 1-day averages), obtained with MOM model using 6-hour meteorological data from NCEP, was provided by J.Staneva. T,S and velocity fields as produced by the MOM model run over the entire Black Sea,

under the same forcing, were also provided in view of their use for initial and boundary conditions in the shelf / high resolution POM model.

a)Wind stress

In the following runs we used 1-day averaged wind stress (Fig. 3). The wind stress patterns (as well as the surface heat fluxes patterns) after an averaging over a 10 days period or a month period, seem quite similar for the 2 different years, probably due to the method used to produce the forcing fields by the MOM model (climatic signal

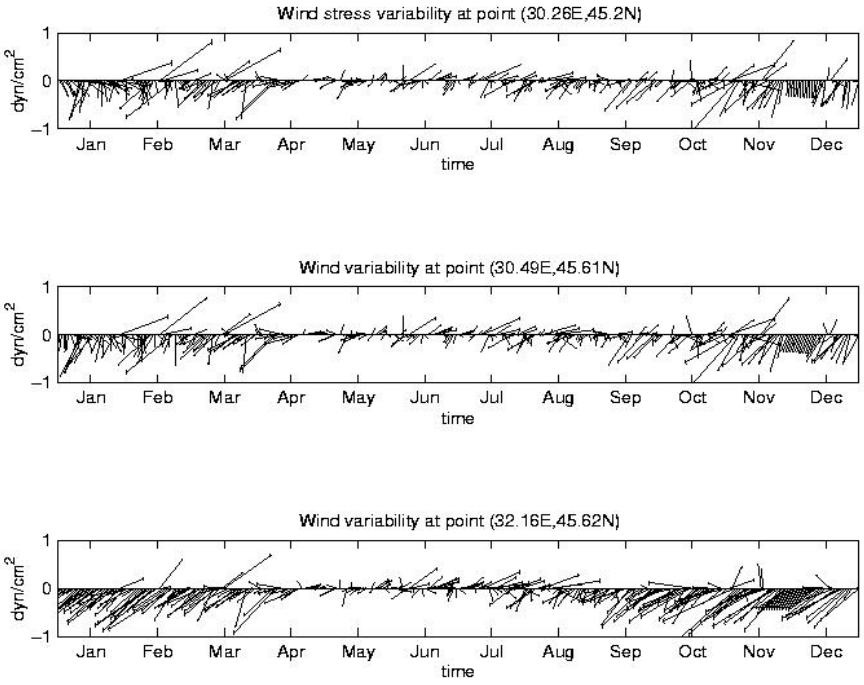

Fig. 3: 10-day averaged wind stress patterns at the middle of every month

added to the high frequency signal). The most important features in the wind stress patterns are as follows.

During winter (December- February) strong prevailing NE winds are observed in the Northwestern shelf. As we can see from the wind stress variability near the Danube River (point 32.16E,45.62N), these winds are almost unchangeable throughout the winter and are expected to cause intense coastal upwelling. The wind in the Danube discharge area is mostly Northern or Northeastern (downwelling favorable). The wind stress curl patterns (not shown) are characterized by a cyclonic structure (positive) with its peak

located west of the Crimean peninsula and extending towards the southwestern direction, while an anticyclone (negative) is located east and sometimes south and southeast of the Danube area. A smaller anticyclone is also observed south of the Crimean Peninsula.

From April until August the wind stress is severely weakened. During May, Jun and July the wind direction becomes Western is the Danube area. In autumn the wind is gradually increasing. The main cyclone is located south of the Crimean peninsula while the anticyclonic structure is covering the largest part of the Northwestern shelf. In general. the wind stress is negative (anticyclonic) in the southern part of the open boundary.

b)Heat fluxes , E-P

We use 10-day averages for the (net) surface heat fluxes. For Solar radiation which is explicitly included in the model, we use monthly mean averages as we do for E-P as well. The surface heat fluxes are fixed (calculated by the MOM model) not allowing for any feedback. As a result the temperature was observed (in some preliminary runs) to reach unrealistic values, especially in very shallow areas. To avoid this, we introduced a relaxation of the surface temperature to the climatological one with a restoring coefficient g=1m/day(~50W/m^2). In forthcoming runs, with 6-hour meteorological data forcing, the heat fluxes will be interactively calculated (using the model SST) from bulk formulas, allowing for feedback which is expected to keep the surface temperature to more reasonable values. Surface salinity is also relaxed towards climatology with a weaker restoring coefficient g=0.5m/day.

c)River Discharge

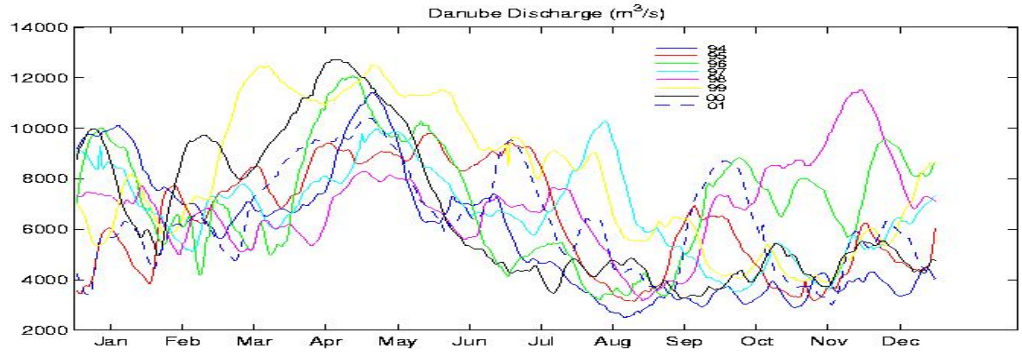

Figure 4. Danube River discharge.

The Danube River runoff variability for the years 1994-2001 is shown in Fig. 4. The data are daily values provided by wp5. An annual average has been calculated and used in the climatological simulations.

Initial Conditions

The T,S fields required for the initial and boundary conditions are obtained from a POM large scale (10Km) run over the entire Black Sea. This run utilizes forcing and climatology relaxation fields calculated by the basin-wide multi-year MOM simulation described in section 4.2. However, it includes plume dynamics and improved description of the hydrographic properties on the Northwestern Black Sea shelf. For the Danube's plume to be more realistically represented in the initial conditions the T,S fields are modified by a 30 day model run with only the river discharge active; the resulting fields are displayed in Fig. 5. Starting time for the simulation is the 1st of April and the duration is 2 years.

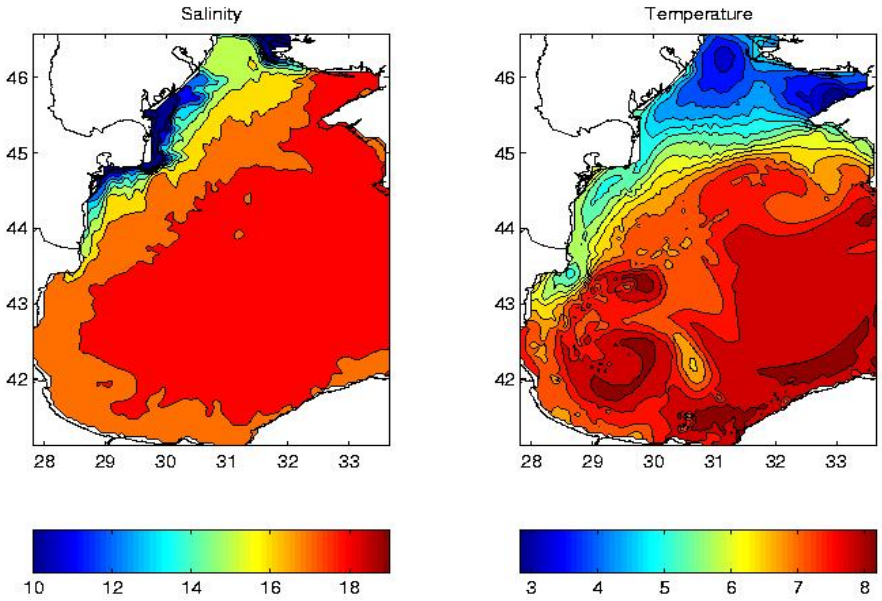

Figure 5: Near surface initial temperature and salinity fields provided by the basin-wide POM run (MOM fields and 30-day river plume run).

Results

During winter, winds are mostly downwelling favorable in the Danube area and the low salinity band is constrained near the coast. In addition, the strong Northeastern

winds are causing intense coastal upwelling along the North Eastern coast which is characterized by an increase of the surface salinity and temperature (the intermediate layer is characterized by S~19 T~9). This high salinity upwelled water is advected towards the Western shelf diminishing the Danube's plume, which is more evident in February-March.

From May until September winds are very week and the Danube's plume is again quite prominent. Summer stratification enables offshore advection of low-salinity waters. On July the western winds blowing in the Danube area are moving the plume towards the east while the resulting upwelling mostly south of the Danube causes an increase of salinity.

A well defined Rim current is observed throughout the year. An anticyclonic structure with south western direction is observed in the summer south of the Danube (Kali-Akra anticyclone) that could be explained by the negative wind stress curl in this area. The Sevastopol anticyclone is also observed throughout the year, but is more pronounced in winter. During May-September an anticyclonic structure is observed in the south corner of the open boundary as induced by the negative wind stress curl in this area.

5. Seasonal distribution of the biogeochemical properties

5.1 Three-dimensional distribution of the biogeochemical properties of the Western Black Sea.

In this section we analyze the model simulations from the on-line coupling between POM and the five-compartment biological model (POM-BIO, Figures Group 4).

In winter phytoplankton concentrations are generally low. Highest values are observed along the north-western coast due to nutrients input from Danube (e.g. 25-30 February). A sharp front is observed between the coastal and the offshore waters in January-February. The area with higher concentration of phytoplankton is very narrow, following the western coast. These high concentrations are triggered by the Danube

nutrient supply. Due to the very small light limitation function in this period of the year, the off-shore area remains uninfluenced by the Danube nutrient supply, hence he concentrations of phytoplankton there are almost negligible. Due to the coastal upwelling mainly in the area north of the Crimean peninsula, which is caused by the strong prevailing north-eastern winds, the phytoplankton concentration is also relatively high. In the area within the cyclonic gyre phytoplankton increases, but in a very low concentration; the same result is also simulated by the model in late winter, early spring. A month later the concentration of the phytoplankton in this area decreases, due to the additional supply of nutrients from below. Several small-scale structures with maximum values of phytoplankton are observed there, which are dynamically caused. In early March the phytoplankton blooms in the north-western shelf. In the period between March to May several major phytoplankton and subsequent mesozooplankton blooms are simulated by the coupled model (see for example the patterns in 5-10 March, 20-25 April, 25-30 April). In March the southward transport is rather weak, due to the antycyclonic circulation in the north part of the shelf, which limits the nutrient supply. This result is also supported by the data obtained from the SeaWiFS images, Barale et al. (2002). These features are much better illustrated in the 5-day averaged patterns, rather than in the monthly-averaged ones. These blooms are mainly due to the high rate of nitrate entrainment together with the large contribution of the light limitation is spring period. The relatively higher chlorophyll concentrations are transported off-shore. The tongue shape formation distributes shelf waters to the deeper basin (e.g. 20-25 May). This phytoplankton bloom terminates two weeks later due to nitrates limitation. In the patterns of 25-30 May several meanders with high chlorophyll concentrations are simulated along the Bulgarian and Turkish coasts. In 20-25 April a core with higher chlorophyll concentrations is simulated along the Danube-plume area. The southward transport increases and the waters rich with chlorophyll are already distributed over the whole Bulgarian coast. From the other side a filament with high chlorophyll concentration is developed from the east boundary of the basin off-shore. The downstream transport from the north-western area of the sea seems to be a very important factor for maintaining a local production along the western and southern coast. This is very well observed in the phytoplankton distribution in 20-25 May. During May highest

phytoplankton values are observed in the south eastern corner as a result of the supply of the surface waters from below due to the upwelling. In summer the bloom of the phytoplankton is predicted in the Danube area. What is typical for the phytoplankton distribution in June is the existence of sharp boundary separating Danube plume waters from the least productive offshore region. This sharp front is connected with the dynamical processes associated with the Danube plume transportation. The water with higher productivity is well traced and remains decoupled from off-shore conditions. These chlorophyll-rich waters are then spread southward either along the cost, or via a separation of the meander west from Crimea peninsula (e.g. 20-25 June). The most prominent feature in this pattern is the intrusion of coastal waters, with higher chlorophyll concentration into the open sea. Similar intrusions are reported by Staneva et al., 2002 and also observed by the SEAWIFS satellite-images. These results demonstrate that the coupled model is capable to simulate small-scale processes connected with the eddy dynamics and meander activities. A month later (end of July and beginning of August) the highest concentration of nutrients is observed at the central area (characterized with cyclonic circulation). Due to mixing processes, the blooms of phytoplankton are simulated along the Bulgarian coast (e.g. 10-15 August), close to the Bosphorus area (10-15 September) and close to the Dnepr River.

In the summer-autumn period several meanders are observed in the horizontal pattern of chlorophyll distribution within the Danube area and the vicinity of Crimea Peninsula. The chlorophyll concentration of the off-shore area is a factor of 5 lower. Some mesoscale and sub-mesoscale structures develop within the south-western area. A well-pronounced fall bloom is simulated along the Danube plume area (e.g. 25-30 September). A second autumn bloom starts in the cyclonic central area of the sea (even with lower concentration). This bloom is due to increase in the mixed layer and the nutrient supply from below. In October the bloom is again located within a very narrow front along the western coast.

We are not going to describe here the seasonal distribution of the zooplankton. It is clear that, due to the grazing pressure, it follows the phytoplankton events and it is strongly supported by the observational data.

In spring, the nitrates concentration in the central part of the sea is very low. High concentrations are observed along the Bosphorus area and west of Crimea, which are caused by physical processes. These high concentrations are further spread along the shelf break to the south-western part of the sea. The water within the Danube-delta area is characterized by high nitrates concentration.

Very interesting features are observed in the pattern of the horizontal distribution of nitrates in the summer period. A sequence of meanders is simulated in the nitrates fields. Several structures with lowest nitrate concentration are distributed in the central part of the basin. These areas almost coincide with the phytoplankon bloom intensification there. Therefore we could claim that the bloom in this area is the result of nutrient limitation rather than due to the supply from the Danube-plume waters. On the other hand, the nutrient content in the Danube area is relatively high, which is due to offshore spreading of Danube induced low salinity waters during this period of the year. In August the area with high nutrient concentrations is located along the shelf break and along the Anatolian coast. An off-shore meander with high nutrient concentrations is also simulated by the coupled model on July. A remarkable filament is observed along the southern coast, transforming nutrient rich waters off-shore (e.g. 15-20 August). Similar structure is also registered by the satellite images. Another interesting structure can be noted in the distribution of nitrates in September. The downstream transport of nutrients is clearly seen at this month. It appears to be a crucial factor for the existence of high chlorophyll content along the whole western and southern coasts. The nutrient-rich waters are transported along the entire Bulgarian and Turkish coasts, reaching the east boundary of the model basin. A wave-structure is observed west of Crimea.

5.2. Evolution of the vertical profiles of the ecological variables

In this section we analyze the model simulations from the off-line coupling of the biogeochemical model ERSEM (Figures Group 5) with the POM-BIO model. In order to include the most important ecological and physical processes associated with the impact of the Danube River this coupling uses the model physics diagnosed by the POM-BIO, mixed layer dynamics (see Section 2.1) and complex ecological model ERSEM (See

Section 3.3). The results are presented as 2-D patterns of the seasonal evolution of some of the model simulated state variables. X-axis corresponds to the time (starting from 1st of January), Y-axis is the depth of water column. The results are illustrated for the 40-th year of integration, when an equilibrium state, with repeated cycle of the dynamics in the "closed" system is achieved.

Here we will analyze the seasonal variability averaged in two areas (shelf **SH** and open-sea one, distinguished with salinity of 17 psu) and two separate locations: **S1** with coordinates (44.4 N, 29.8W) and **O1** with coordinates (43.8 N, 32 W).

A sequence of surface blooms is simulated through the annual cycle in all patterns. The first peak of the phytoplankton is controlled by nitrates and phosphates. The maximum of total phytoplankton during the first winter spring blooms varies between 1.2 mg Chl a. m^{-3} in the offshore region and above 3 mg Chl a. m^{-3} in Danube plume area. Since in this period (late winter, early spring) the mixed layer is a maximum, this bloom is observed within the upper 50 meters of the water column. The first diatom bloom is not controlled by Zooplnkton grazing. It is determined by the limitation of phosphate: The phytoplankton reach their maximal concentrations when the phosphate is limited! This result is supported by observational evidence (A. Cociasu, personal communication), as well as by the numerical simulations, performed with BIOGEN model (Lancelot at el., 2002). Due to the lack of predator grazing (micro- and meso-zooplankton abundance in this period), these blooms are easily triggered by the small increase by the light limitation. If we compare the results in coastal and open areas, we can see that the chlorophyll concentration of diatoms is about a factor of three higher in the enrichment ecosystem. This result visually coincides will the images, obtained from the satellite data (Barale e al., 2002), as well as from the observations. The periods for those blooms differ in the different areas of the sea: the spring bloom lasts about 20 days for the area averaged shelf zone **SH**, in **S1** area it is simulated earlier and lasts about 15 days, while in **O1** area it occurs only for 5 days. About a week later (at the beginning of April), the phytoplankton disappears either by lysis or by sedimentation. Diatom-derived organic matter stimulates Bacteria growth. Its maximal concentration (of about 30 mg C. m^{-3}) coincides very well with the values obtained from the measurements. Thus, the model is already tuned sufficiently well to reproduce not only good seasonal characteristics of the

biogeochemical variables, but to keep their concentrations close to what is known from previous studies in the Black Sea. Here we would like to remind that the modeling study within the DANUBS project is the first Black Sea application of such a complex moduled ecological model as ERSEM. During the peak of Bacteria, the diatoms, micro-zooplankton and copepods are kept in very low concentrations. In such a way Bacteria plays a key role in the system by outcompeting diatoms in PO4.

Several secondary phytoplankton blooms occur shortly after the first bloom during different periods of the year: through the full summer for **S1**, mainly in August for **SH1,** while for the open area and location a sequence of blooms is predicted very shortly after the first one takes place in spring and early summer. These blooms are simulated by phosphate/nitrate regeneration by bacterial activity, which is related to the regenerated production. Some of these blooms are due to the strong grazing pressure of micro-zooplankton, which peaks in the summer period. This peak is controlled by the mezo-zooplankton. The maximum concentration of micro-zooplankton is about 30 mg C. m^{-3}, for the Danube-influenced waters, while in the offshore area the micro-zooplankton has a maximum of about 16 mg C. m^{-3}. This result correlates very well with the observations. The biomass of the macro-zooplankton exceeds that of the micro-zooplankton in the open area (having its first maximum in June and a stronger peak from mid-September until the end of November). The concentration of meso-zooplankton is Danube plume area (SH) is very high (of about 35 mg C. m^{-3}) in June. This result is supported by observational evidence.

Through the rest of the year the biomass of the macro-zooplankton at the sea surface in SH area is very slow. At the layer of 30-50 a high concentration of macro-zooplankton is predicted starting from June until the end of the year. The shape of the macro-zooplankton distribution in the evolution of the vertical column resembles that of the mixed-layered depth. In the period from February to April the water column suffers from the lack of macro-zooplankton. A very interesting feature is simulated in the evolution of the macro-zooplankton in **S1** area. A core with a maximum macro-zooplankton is simulated in August-September at the layer between 30 and 50 m. This core is dynamically caused. It results from waters that were advected laterally. Similar features cannot be simulated by a simple one-dimensional coupled model only.

Subsurface distributions, which have advective origin are also observed in the evolution of the phytoplankton depth in OP area. The second peak of Bacteria in **SH** is much stronger than the first one (about 16 g C. m^{-3}).

Several subsurface maxima of phytoplankton are simulated through the seasonal cycle, which are due to the supply of nutrient rich waters from below, together with sufficient light availability. In the fall, when the vertical mixing starts to be stronger again, a bloom appears in the open area **OP**. It is also important to note here that in the model predictions silicate is never lower than nitrates. This result is consistent with the observational evidence (A. Cociasu, personal communications). Because of the strong stratification the surface layers can not be supplied with high concentrations of NO3, PO4 and Si(OH) from enriched layers below 60 meters and the strong gradients are observed at these depths.

A general agreement is observed between model predictions and what we know from literature data, both in seasonality and in magnitude. The maximum concentrations of nitrates, phosphorus and silicate in the shelf area **SH** are in winter and are 30, 4.1 and 12 mg C. m^{-3}, respectively. In the simulations in the "coastal area", similar to the previous ones, silicate is never lower than nitrates. The concentration of nitrates, phosphate and silicate increases rapidly below the thermocline. This result is supported by observational evidence.

5.3 Basin-scale biogeochemical results

Here we will show the results from the basin-scale coupled physical-hydrological model. Since we are mainly interested on the role of the physical processes (such as different ocean fronts, waves, meanders and eddies) of the phytoplankton dynamics, the results will be presented as shorter than a monthly averaged (Figures Group 6).

The upper layer thermal state, particularly in winter, governs the formation of cold water that can be used to analyse the correlation between the simulation and observations. We show on Fig. 5.3.1 the horizontal patterns of the model simulated sea surface temperature and the ones obtained from infra-red (AVHRR) images in spring (MAM) and fall (SON). The coldest temperature is observed in the northwestern part of the sea. The temperature increases southeast having maximal values in the southeastern part of

the sea in spring and fall (about 12 ^{o}C and 20 ^{o}C, respectively). The following conclusions can be made from these comparisons: (1) There is a close correlation between the horizontal patterns of simulated and satellite data. (2) The atmospheric data (not shown here) are smoother that is associated with the coarser resolution, as well as with the different length scales in both data types. (3) The warm tongues in the southern and eastern Black Sea are dynamically caused (this pattern is not as pronounced in the atmospheric temperature). The agreement between the temperatures simulated by the model and obtained from the AVHRR data demonstrates that the model resolves very well both the circulation patterns and the temporal and spatial variability of temperature. As we will demonstrate below this is of crucial importance to the correct simulation of the biogeochemical characteristics in the Black Sea. The model temperatures are lower than observed that is due to the strong cooling of the shelf and perhaps to the insufficient amount of AVHRR observations to produce reliable averaging. Obviously, the small scale patterns in the observations prove that the model resolution is still insufficient to resolve small scales. However, complete correlation between the two data types is not to be expected since we do not integrate the model in assimilation mode.

Some snapshots of model simulated chlorophyll-a and sea surface temperature during May are shown on Fig. 5.3.2. The sharp boundary separating the high chlorophyll coastal waters from the basin interior is clearly observed. The Danube river plume is narrow and is concentrated along the Danube-delta region. The maximum chlorophyll-a concentration in March is about 4 mg/m^3 and is located close to the Danube area. In the basin interior the chlorophyll-a concentration is very low. Several intrusions of chlorophyll-rich coastal waters from the southern coast supply the central areas of the sea.

The horizontal patterns of chlorophyll-a 10-15 June 5-10 August simulated by the fine resolution model are shown on Fig. 5.3.3 and 5.3.4, respectively. In June all shelf area is filled with rich of chlorophyll waters (with a concentration of about mg/m^3). This water is further spread southward along the western coat reaching the southernmost part of the sea. Then, due to the intrusions of the Bosphorus plume, it is distributed further in eastern direction as well as into the basin/interior. In both simulations the interior of the basin, characterized by a cyclonic circulation and higher salinity (due to the cyclonic

circulation), the simulated chlorophyll is very low. The frontal zone between the high and low chlorophyll distribution is located at about 100 m isobath. Several meanders are also simulated by the model. The tongue-like meander formed along the southern coast introduces high chlorophyll waters at about 200 km into the interior of the sea. The fresh-and-cold-water system penetrates south-westward along the western Crimean coast. The relatively higher chlorophyll concentration inside this filament is transported offshore. One meander is separated from the filament transporting coastal waters in the shelf slope. Similar distribution of filaments and meanders along the Crimean coast was also simulated by Staneva et al., (2001). Along the eastern coast there is very narrow area with high concentration. In the second period (5-10, August, see Fig. 5.3.4) the Danube River plume is very narrow. It flows downstream along the Bulgarian and Turkish coast, separating both types of waters with a very sharp frontal area. The offshore transport associated with the Bosphorus plume is clearly observed. Several filaments and eddies are also simulated between the southern coast and the Rim current, exporting large proportion of coastal waters into the interior of the basin with still higher concentration (about 2 mg/m^3).

The consequence of monthly averaged chlorophyll distributions at the sea surface is presented at Fig. 5. A strong seasonal and spatial variability is observed through the year. The patterns are much smoother compared with the previous results. This is due to the coarse resolution of the model and also to the time-averaging. All meanders and small-scale eddy-features disappear in these patterns. In winter-autumn months the Danube River plume is restricted mainly near the Danube delta. In the open area the chlorophyll concentrations are minor.

The northwestern part is totally occupied by high chlorophyll waters. These waters spreads southward along the western cost and it is further introduced into the basin interior manly in summer seasons. Several blooms are observed in the north-western part of the sea. In winter-autumn those blooms are mainly located close to the Danube delta, while in fall-summer some blooms take place either northward or southward of the delta. In December and February chlorophyll concentration tends to decrease. The north-western coastal waters remain productive during all months. This is due to the supply of nutrients from the Danube as well as of increasing the mixed layer depth in cold part of

the year. Similar behavior is also observed in the SEAWIFS images analysed in details by Oguz et al., 2002. The biological activity is stronger in spring-summer. The horizontal patterns provide a good example that the north-west area of the sea provides the western and southern coasts with high-productivity water. The frontal areas are also well expressed.

6. Conclusions

We analyzed the seasonal distribution and variability of the physical and biological component simulated by a hierarchy of models. We demonstrated that the components of the biological pump are very sensitive to the vertical variability of light, mixed layer depth, nutrients, etc. According to Longhurst (1981) the horizontal dimension is a second property of the oceanic biological system. Therefore, when studying the biological cycle in the upper layers one has to start with vertically resolved models, since they take into account the vertical structure not only of light, but also of turbulence and nutrients (Radach and Moll, 1993).

The model estimated monthly air-sea heat, fresh water and momentum fluxes, using atmospheric analyses data and bulk parameterizations are consistent with climatological estimates for the Black Sea region. The surface forcing data set is coupled with the model ocean and the resulting simulations quantitatively reproduce much of the observed behavior of the horizontal and vertical characteristics, such as the formation of cold intermediate layer, heat content, annual cycle of the mixed layer depth. In this high frequency data set the air-sea fluxes of heat and momentum depend on the model simulated Sea Surface Temperature (SST). According to Doney a reasonable strong case can be made for the utility of operational numerical data in the upper ocean numerical studies, particularly when no other representative alternative exists. Single events caused by the weather are prone to be very important in the transfer of matter during the annual cycle. Rapid changes of the physical environment occur on the time scales of days, which are the same scales as the time characteristics of the plankton system.

The environment of nutrients across the thermohaline into the mixed layer is highly variable. Thus the amount of nutrients entrained will show seasonally different patterns and varying effects on the plankton dynamics, even if the integrated variability will

remains the same between the years. This seasonal cycle, illustrated in the behavior of the biological system, is strongly controlled by the seasonal variability of the physical processes. The impact of upper layer physics on the biological systems is addressed in a number of studies (Wolf and Woods, 1988; Radach and Moll, 1993). Goldman et al. (1988) found that fifty percent of the variance in the interannual variability of the primary production can be attributed to the spring weather conditions, proving that meteorological factors are of the utmost importance for the interannual variability. Primary production is considerably affected by the short-periodic meteorological events (Radach and Moll, 1993).

The performance of the coupled 3D ecological model will be further validated with the simulation of specific periods that will be chosen based on data obtained during the daNUbs project. This will be done within the next two years of the project. The climatological model predictions show that the euthrophication-related problem is a question of changes in the nutrient balance, not only qualitatively, but also quantitatively. Whether the phosphates or nitrates are limited depends strongly on this balance. The present coupled model simulations confirm the key role of PO4 in euthrophication related phenomena. The coupled physical and biogeochemical model, which is very well calibrated for the Black Sea conditions, allows us to test different scenarios, regarding the structure of the ecosystem as a function of meteorological and human forcing. The model can be used for the performance of simulations that are of interest for both scientists and policy makers and can be used for management purposes.

References

Barale, V., Cipollini, P., Davidov, A. and Melin, F. , (2002). Water constituents in the north-western black sea from optical remote sensing and in situ data. Estuar. Coastal and Shelf Sci., 54, 309-320.

Baretta, J. W., W. Ebenhoeh, and P.Ruardji, (1995). Regional Seas Ecosystem Model (ERSEM), a complex marine ecosystem model. Neth. J. Sea Res., 33, 233-246.

Baretta-Bekker, J.G., L.W. Baretta, and E.K. Rasmussen, (1997). The microbial food web in the European Regional Ecosystem Model. Neth. J. Sea Res., 33, 33-379.

Besiktepe, S.T., C.J. Lozano and A.R. Robinson, (2001). On the summer mesoscale variability of the Black Sea Journal of Marine Research, 59, 475-515.

Beckers, J. M., M. L. Gregoire, J. C. J. Nihoul, E. Stanev, J. Staneva and C. Lancelot, (2002). Modelling the Danube-influenced Nort-western continrntal shelf of the Black Sea. I: Hydrodynamic processes simulated by 3-D and box models. Estua. Coast and Shelf Sci., 54, 453-472.

Berliand, M. E. and T. G. Berliand. (1952). Measurement of the effective radiation of the Earth with varying cloud amounts. Izv. Akad. Nauk SSSR, Ser. Geofiz.*,* ***1*****,** 64-78, (in Russian).

Blackford, J.C., and P.J. Radford, (1997). A structure and methodology for marine ecosystem modelling. Neth. J. Sea Res., 33, 247-260.

Blumberg, A.F. and G.L. Mellor, (1983). Diagnostic and prognostic numerical circulation studies of the South Atlantic Bight. *J. Geophys. Res*., **88(C8)**, 4579-4592.

Broekhuizen, N., M.R. Heath, S.J. Hay, W.S.C. Gurney, (1997). Predicting the dynamics of the North Sea's mesozooplankton. Neth. J. Sea Res., 33, 381-406.

Bryan, K. (1969). A numerical method for the study of the circulation of the World Ocean. J. of Computational Physics, *4*, 347-378.

Bryant, A.D., M.R. Heath, N. Broekhuizen, J.G. Ollason, W.S.C. Gurney and S.P.R. Greenstreet, (1995). Modelling the predation, growth and population dynamics of fish within a spatially-resolved shelf-sea ecosystem model. Neth. J. Sea Res., 33,

407-421.

Ebenhöh, W., (1997). Microbial dynamics in the marine ecosystem model ERSEM II with decoupled carbon assimilation and nutrient uptake. J. Sea Res., 38.

Ebenhöh, W., J.G. Baretta-Bekker, and J.W. Baretta, (1997). The primary production module in the marine ecosystem model ERSEM II, with emphasis on the light forcing. J. Sea Res., 38,173-193.

Fasham, M., H. Ducklow and S. McKelvie (1990). A nitrogen-based model of plankton dynamics in the oceanic mixed layer. J. Mar. Res., **48**, 591-639.

Goldman, C.R., A. Jasby and T. Powell (1990). Interannual fluctuations in primary production: Meteorological forcing at two subalpine lakes. Limnology and Oceanography, 34, 308-321.

Gregoire, M. J.-M. Beckers, J. C. J. Nihoul, and E. Stanev, (1997). Reconnaissance of the main Black Sea ecohydrodynamics by means of a 3D interdisciplinary model, J. Mar. Sys., 16, 85-105.

Gregoire, M, J.-M. Beckers, J. C. J. Nihoul, and E. Stanev, (1998). Simulation of the annual plankton productivity cycle in the Black Sea with 3D high resolution interdisciplinary model, In: ECCOMAS 98, 461-464. John Wiley and Sons Publ.

Gill, A. and J. S. Turner, (1976). A comparison of seasonal thermocline models with observations. Deep Sea Res. 21, 391-401/

Gordon, C. and M. Bottomley, (1985). The parametrization of the upper ocean mixed layer in coupled ocean-atmosphere models. In: J.C.J. Nihoul (editor), coupled ocean-atmosphere models. (Elsevier Oceanography Series, 40), Elsevier, Amsterdam, 613-637.

Hellerman, S., Rosenstein, M., 1983. Normal monthly wind stress over the world ocean with error estimates. J. Phys. . Oceanogr. 13, 1093-1104.

Ivanov, L I., S. Besiktepe, and E. Ozsoy, (1997). The Black Sea cold intermediate layer. in E. Ozsoy and A. Mikaelyan (eds.), Sensitivity to change: Black Sea, Baltic Sea and North Sea, NATO ASI Series, Vol. *27*, Kluwer Academic Publishers, 253-264.

Kourafalou, V.H., L.-Y. Oey, J.D. Wang and T. N. Lee**,** (1996a). The fate of river discharge on the continental shelf. Part I: modeling the river plume and the inner-shelf coastal current. *J. Geophys. Res.*, **101(C2)**, 3415-3434.

Kourafalou, V.H., L.-Y. Oey, T. N. Lee, and J. D. Wang**,** (1996b). The fate of river discharge on the continental shelf. Part II: transport of coastal low-salinity waters under realistic wind and tidal mixing. *J. Geophys. Res.*, **101(C2)**, 3435-3455.

Kourafalou, V.H., (1999). Process studies on the Po River plume, North Adriatic Sea. J. Geophys. Res., **104(C12)**, 29963-29985.

Kourafalou, V.H. (2001). Modelling river plumes on Mediterranean shelves: Po River plume (North Adriatic Sea) and Axios River plume (North Aegean Sea). *J. Marine Syst.,* 30(3-4), 181-205.

Lancelot, C. L., J. V. Staneva, D. Van Eeckhout, J.-M. Beckers, and E. V. Stanev (2002), Modelling the Danube-influenced North-western continental shelf of the Black Sea. Ecosystem response to changes in nutrient delivery by the Danube River after its damming in 1972. Estua. Coast and Shelf Sci., 54, 473-499.

Lewis, B. L. and W. N. Landing, (1991). Manganese and iron in the Black Sea., Deep Sea Res*., 38*, S773-S805.

Longhurst, A.R. 1981. Analysis of marine ecosystems. Academic Press, Nueva York. 741 págs + xxii. (574.52636 A532)

Mellor, G. L. and Yamada, T., (1982). Development of a turbulence closure model for geophysical fluid problems. Rev. Geophys. Space Phys., 20, 851-875.

Oguz, T., E. Özsoy, M. A. Latif, H. I. Sur, and U. Unluata. 1990. Modeling of hydrographically controlled exchange flow in the Bosphorus Strait, J. Phys. Oceanogr. *20*, 945-965.

Oguz, T., D. Aubrey, V. Latun, E. Demirov, L. Kolesnikov, H. Sur, V. Diaconu, S. Besiktepe, M. Duman, R. Limeburner and V. Eremeev, (1994). Mesoscale circulation and thermohaline structure of the Black Sea during HydroBlack'91, Deep Sea Res., *41*, 603-628.

Oguz, T., H. Ducklow, P. Malanote-Rizzoli, S. Turgul, N. Nezlin and U. Unluata,

(1996). Simulation of annual plankton cycle in the Black Sea by a one-dimensional physical biological model. J. Geoph. Res., 101, 16551-16569.

Oguz, T., P. Malanote-Rizzoli, and H. Ducklow, (2001). Simulation of plankton seasonal cycle with multi-level and milti-layer physical-ecosystem models: The Black Sea example, Ecological Modelling, 144, 295-314.

Oguz***, T***., Ashwini G. Deshpande and P. Malanotte-Rizzoli (2002) "On the Role of Mesoscale Processes Controlling Biological Variability in the Black Sea: Inferrences From SeaWIFS-derived Surface Chlorophyll Field". Continental Shelf Research*,* 22. 1477-1492

Ovchinnikov, I. M. And Yu. I. Popov. (1987). Evolution of the Cold Intermediate Layer in the Black Sea. Oceanology, *27*, 555-560.

Ovchinnikov, I. M., (1998). Interaction between surface and deep waters in the process of transverse circulation of the Black Sea. In: Ventilation of Black Sea Anoxic Waters. Workshop Rep. Ser., 1/05/98, Liege, 135-161.

Pacanowski, R. C., K. Dixon and A. Rosati, (1991). The GFDL Modular Ocean Model Users Guide, version 1.0. GFDL Ocean Group Tech. Rep., No 2, 176 pp.

Paulson, C.A. and J.J. Simpson, (1977). Irradiance measurements in upper ocean. J. Phys. Oceanogr., 7, 952-956.

Radach G. and A. Moll, (1993). Estimation of the variability of production by simulating annual cycle of phytoplankton in the central North Sea, Progr. Oceanogr., 31, 339-419.

Rosati, A. and K Miyakoda, (1988). A general circulation model for the upper ocean simulation. *J. Phys. Oceanogr*., **18**, 1601-1626.

Saydam C., S. Tugruk, O. Basturk and T. Oguz, (1993) Identification of the oxic/anoxic interface by isopycnal surfaces in the Black Sea. Deep-Sea Research, 40, 1405-1412.

Sorkina A.I. (Ed.), 1974. Reference Book on the Black Sea Climate, Moscow, Gydrometeoizdat, 406 pp. (in Russian).

Stanev, E. V., (1990). On the mechanisms of the Black sea circulation. *Earth-Science Rev*., **28**, 285-319.

Stanev, E.V, J.V. Staneva and V.M. Roussenov, (1997). On the Black Sea Water Mass Formation. Model Sensitivity Study to Atmospheric Forcing and to Parameterizations of some Physical Processes. *J. Mar. Sys.*, 13, 245-272.

Stanev, E.V., and J.V. Staneva, (2000). The impact of mesoscale eddies in the transitions of quasistable states in the circulation of the Black Sea. Ch. Mooers (editor), Special Issue in *J. Mar. Sys.,* 24, 3-26.

Staneva J. V., E. V. Stanev and N. H. Rachev, 1995. Heat balance estimates using atmospheric analyses data: A case study for the Black Sea. *J. Geophys. Res*., **100**, 18581-18596.

Staneva, J.V. and E.V. Stanev (1997). Cold water mass formation in the Black Sea and its sensitivity to horizontal resolution in numerical models. E. Ozsoy and A. Mikaelyan (eds.): *Sensitivity of North Sea, Baltic Sea and Black Sea to anthropogenic and climatic changes*, NATO Series, Kluwer academic publisher; 375-393.

Staneva J. V. and E. V. Stanev and T. Oguz, (1998). The Impact of Atmospheric Forcing and Water Column Stratification on the Yearly Plankton Cycle, In: T. Oguz and L. Ivanov (eds.) NATO-ASI Kluwer academic publisher, 301-323.

Staneva J.V., and E.V. Stanev, (1998). Oceanic Response to Atmospheric Forcing Derived from Different Climatic Data Sets.Intercomparison Study for the Black Sea. Oceanol. Acta, 21, 393-417.

Staneva, J. V., D. Dietrich, E. Stanev, and M. Bowman, (2001). Rim current and coastal eddy mechanisms in an eddy-resolving Black Sea general circulation model. J. Mar. Sys.3, 137-157.

Staneva, J. V. and E.V. Stanev, (2002). Water mass formation in the Black Sea during 1991-1995. J. Mar. Sys., 32, 199-218.

Turgul, S., O. Basturk, C. Saidam, and A. Yilmaz, (1992). Changes in the hydrochemistry of the Black Sea inferred from water density profiles, Nature, 359, 137-139.

Van Eeckhout, D. and Lancelot, C., **(**1997). Modelling the functioning of the North-Western Black sea ecosystem from 1960 to present. *NATO-ASI series* In: E. Ozsoy and A. Mikaelyan (eds). Sensitivity to Change: Black Sea, Baltic Sea and North Sea **2 (27),** 455-468.

Varela, R. A., A. Cruzado, J.E. Gabaldon, (1995). Modelling primary production in the North Sea using European Regional Seas Ecosystem Model. Neth. J. Sea Res., 33, 337-361.

Unluata, U., T. Oguz, M. A. Latif and E. Ozsoy, (1989). On the physical oceanography of the Turkish Straits. in The Physical Oceanography of Sea Straits, NATO ASI Ser., Ser. C, edited by G. Pratt, pp 25-60, Kluver Academic, Norwell, Mass.

Wolf K. an J. Woods, (1988). Lagrangian simulation of primary production in the physical environment-in deep chlorophyll maximum and nutricline. B.J. Rothschild (editor): Towards a Theory of Biological-Ohysical Interactions in the World Ocean. Kluwer Academic Publishers, NATO-ASI Series, 239, 51-70.

Tables

TABLE 1: Characteristics of the wp8 numerical models and simulations

Model name	**MOM-BIO**	**POM-BIO**	**MLD-ERSEM**
Model type	3-D hydrodynalical (MOM) coupled with low trophic ecological (Fasham)	3-D hydrodynalical (POM) coupled with low trophic ecological (Fasham)	1-D (MLD) coupled with low trophic ecological (ERSEM)
Model geographical area	Black Sea	North-western shelf (NWS)	North-western shelf (NWS)
Resolution	9 km	5 km	Box
Vertical discretization	z-coordinate, 24 vertical levels	Sigma-coordinate, 16 sigma levels	z-coordinate, 40 vertical levels.
Surface fluxes	Diagnosed by the model from the atmospheric analyses data , model surface data and flux parameterization	taken from MOM-BIO	taken from MOM-BIO
Initial Condition	Climatological	MOM-BIO	POM-BIO
River fluxes	Climatological	DANUBS (Cociasu)	DANUBS(Cociasu)
Section with model description of the physical part	2.3 (MOM)	2.2 (POM)	2.1 (MLD)
Section with model description of the ecological part	3.1 (Fasham 5-compartment)	3.1 (Fasham 5-compartment)	3.2 (ERSEM, complex 5-moduled)
Section with model physical results	4.2	4.3	4.1
Section with model bigeochemical results	5.3	5.1	5.2

Figures

Group 1 Figures: Mixed-Layered Dynamics: The performance of the 1-D physical model

Group 2 Figures: Seasonal distribution of the physical properties diagnosed by the basin scale 3-D hydrodynamic model MOM

Group 3 Figures: Upper panels: Monthly averaged near-surface salinity and velocity patterns for the western Black Sea, calculated by the fine resolution, western Black Sea POM model. Lower panels: Monthly averaged wind field and near-surface salinity patterns for the entire Black Sea, calculated by the coarse resolution, Black Sea POM model.

Group 4 Figures:

a) Selected 5-day averages of near-surface nutrient distributions on the western Black Sea
b) Monthly averages of near-surface nutrient distributions on the western Black Sea
c) Selected 5-day averages of vertical nutrient distributions over across-shelf and along-shelf sections near the Danube River.

Group 5 Figures: Evolution of the vertical profiles of the ecological variables: model simulations with ERSEM.

Group 6 Figures: Basin-scale coupled physical-hydrological model